Transport Phenomena in Chaotic Laminar Flows

Pavithra Sundararajan[1] and Abraham D. Stroock[2,3]

[1]Sibley School of Mechanical and Aerospace Engineering, [2]School of Chemical and Biomolecular Engineering, and [3]Kavli Institute at Cornell for Nanoscale Science, Cornell University, Ithaca, New York 14853; email: ps333@cornell.edu, ads10@cornell.edu

Annu. Rev. Chem. Biomol. Eng. 2012. 3:473–96

First published online as a Review in Advance on April 23, 2012

The *Annual Review of Chemical and Biomolecular Engineering* is online at chembioeng.annualreviews.org

This article's doi:
10.1146/annurev-chembioeng-062011-081000

1947-5438/12/0715-0473$20.00

Keywords

chaos, mixing, dispersion, interfacial mass transfer, sampling

Abstract

In many important chemical processes, the laminar flow regime is inescapable and defines the performance of reactors, separators, and analytical instruments. In the emerging field of microchemical process or lab-on-a-chip, this constraint is particularly rigid. Here, we review developments in the use of chaotic laminar flows to improve common transport processes in this regime. We focus on four: mixing, interfacial transfer, axial dispersion, and spatial sampling. Our coverage demonstrates the potential for chaos to improve these processes if implemented appropriately. Throughout, we emphasize the usefulness of familiar theoretical models of transport for processes occurring in chaotic flows. Finally, we point out open challenges and opportunities in the field.

INTRODUCTION

Laminar flows are boring: viscous forces dominate inertial ones such that dynamics are quasi-static; no motion occurs spontaneously, that is, without continuous application of force. Laminar flows are also inefficient: steady, parallel streamlines mean that transfer of energy, mass, and momentum within the flow must occur by molecular conduction or diffusion. However, laminar flows are reliable: their quasi-static nature means that, unlike in turbulence, the fluid responds in a deterministic manner to forcing. Furthermore, laminar flows are inevitable: the competition between viscosity and inertia favors viscous forces when the dimension of the flow is small or the viscosity of the fluid is large. In common scenarios found in technology—packed columns, microfluidic reactors, boundary regions in macroscopic systems—the characteristic dimension is small enough that flows of common solvents remain laminar. An important engineering challenge is to make laminar flows more efficient (and perhaps more interesting too!) for transport processes while benefiting from their simplicity and reliability and retaining compatibility with relevant technological contexts. In this review, we consider this challenge in the context of the four fundamental transport processes illustrated in **Figure 1**: mixing (**Figure 1*a***), interfacial transfer (**Figure 1*b***), dispersion (**Figure 1*c***), and spatial sampling (**Figure 1*d***).

CHAOTIC FLOWS

One means to approach the goal of improving transport processes in laminar flows emerged in the 1960s when Arnold (1) identified a class of steady, 3D flows in which the trajectories of fluid elements displayed chaotic dynamics (2). Subsequently, Aref (3) clarified the relationship between these chaotic trajectories in a flow and the chaotic dynamics known in mechanical systems [for example, the double pendulum (4)], and showed that time-dependent, 2D flows could also exhibit chaos.

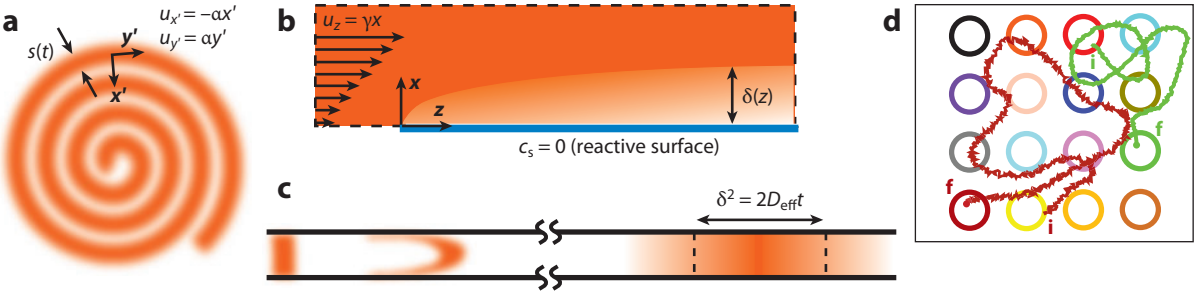

Figure 1

Schematic representations of laminar transport in four contexts. (*a*) Mixing: deformation and diffusion of a solution of solute (*orange*) in a vortex. A simple understanding of mixing is achieved by observing the process in a Lagrangian reference frame (x', y') that moves and reorients with striations in the concentration distribution. The evolution of the width of the band $s(t)$ depends on the local extensional velocity field $u_{x'}$,$u_{y''}$ with an effective strain rate α (5). (*b*) Interfacial mass transfer: convection and diffusion of solute in a shear flow (u_z) past a reactive surface. Mass transfer is visualized as transport of solutes from the bulk through a concentration boundary layer of thickness $\delta(z)$ to the reactive surface with surface concentration $c_s = 0$. γ is the strain rate in the shear flow. (*c*) Taylor dispersion: a band of solute deforms rapidly in a Poiseuille flow until diffusion homogenizes the distribution of solute in the cross section; further axial broadening occurs in a diffusive manner with an effective diffusivity, D_{eff}, that depends on both molecular diffusion and flow speed (62). (*d*) Sampling: solutes undergo convection and diffusion over a surface that is patterned with discrete regions that display specific binding sites. The trajectories of two solutes of distinct type are shown as they travel from initial positions (i) to eventual binding events (f) on their specific regions.

So, chaos sounds interesting, but what does it mean in the context of transport processes? The hallmark of dynamical chaos is the so-called sensitivity to initial conditions, or, more precisely, the exponential separation in time of neighboring trajectories in the phase space (4). In the context of a flow, the phase space is the real space occupied by the flow, and the exponential separation corresponds to exponential stretching of volumes of fluid within the flow. This behavior is captured in one of the simplest possible flows, pure extension (**Figure 2*ai***). To make this flow bounded, we

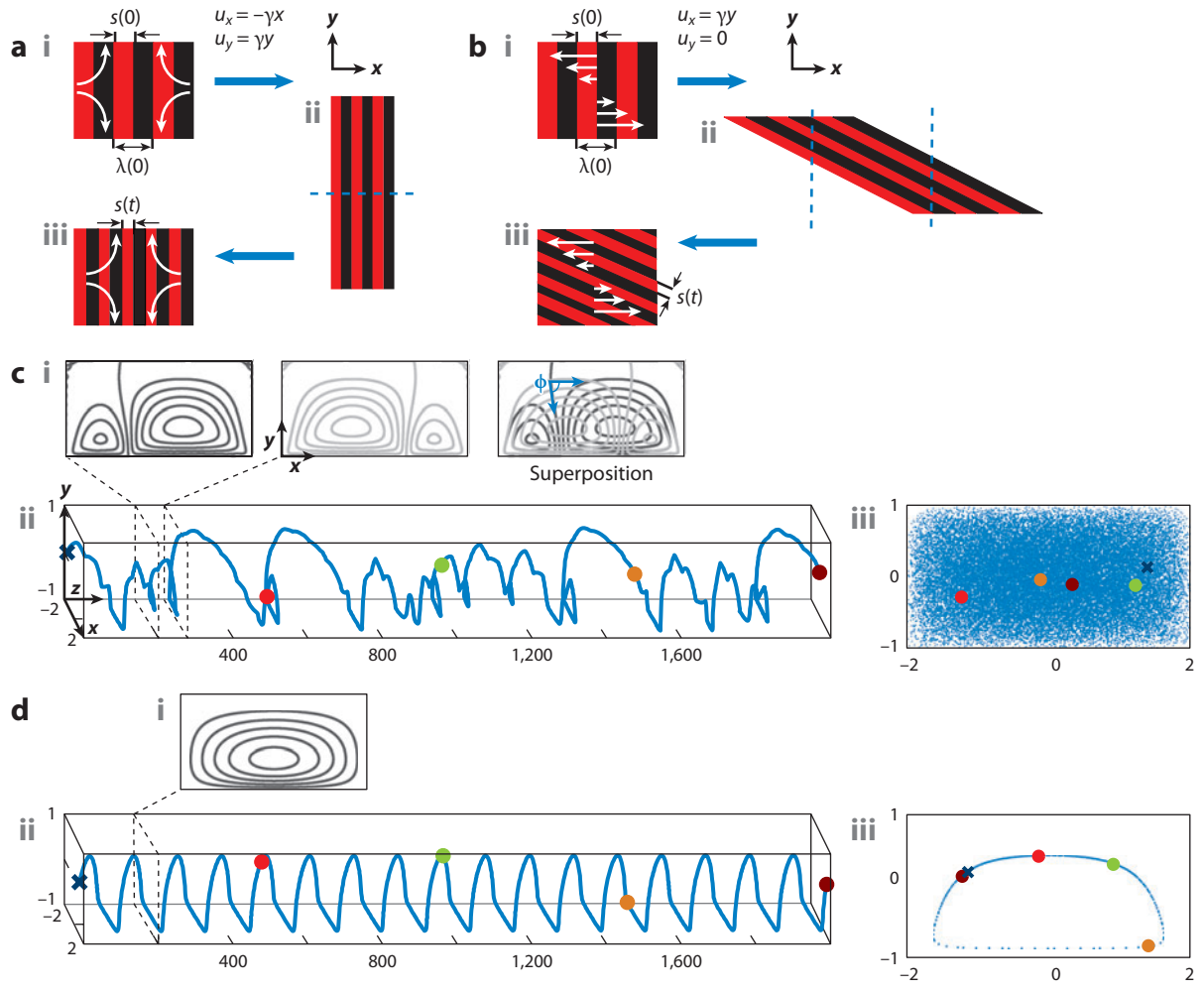

Figure 2

Chaotic and nonchaotic laminar flows. (*a*,*b*) Baker's transformations: Idealized stirring processes achieved with repeated sequences of (*i*) deformation in a linear flow, (*ii*) cutting, and (*iii*) reassembly. (*a*) Pure extension captures the characteristic exponential stretching that occurs in chaotic flow. (*b*) Simple shear captures the power law stretching observed in nonchaotic flows. (*c*,*d*) (*i*) Streamlines of secondary transverse flow, (*ii*) trajectories of nondiffusive tracers, and (*iii*) Poincaré maps in a (*c*) chaotic and a (*d*) nonchaotic duct flow (6). (*ci*, *left and middle*) In panel *c*, the transverse secondary flow switches between two velocity profiles. (*ci*, *right*) A superposition of the streamlines shows the streamline crossing necessary to produce chaotic trajectories. (*ciii*, *diii*) The Poincaré map was generated by recording the positions of a nondiffusive particle (starting at the location marked by ×) at cross sections spaced by 40*H* units, where *H* is the height of the channel. (*ciii*) Twenty thousand positions were recorded in the chaotic case; (*diii*) 400 frames were recorded in the nonchaotic case.

can periodically halt the extension, cut along the contractile axis (**Figure 2*aii***), and reassemble the fluid into its original geometry (**Figure 2*aiii***). This process mimics the manipulation of dough by a baker and is thus called a baker's transformation. The extensional baker's transformation provides a useful model flow with which to consider the impact of chaos on transport processes. We can similarly construct a shearing baker's transformation by deforming the fluid with simple shear, cutting it, and reassembling it (**Figure 2*b***). As suggested by Ranz (5), this shear deformation can serve as a simple model of general, nonchaotic flows. Importantly, these models capture the distinct evolution of the characteristic distance, $s(t)$, over which diffusion must act to eliminate differences in concentration or temperature. In pure extension, $s(t)$ decreases exponentially with time; in simple shear, $s(t)$ varies algebraically with time, with decreasing rates. This distinct evolution leads to dramatic differences in the rates of mixing in chaotic and nonchaotic laminar flows and also leads to subtler but important differences in rates of interfacial transfer.

A second defining characteristic of chaos is the manner in which trajectories explore regions of the flow's domain. **Figure 2*cii*,*dii*** present trajectories of nondiffusive tracers in steady duct flows that are chaotic (**Figure 2*c***) and nonchaotic (**Figure 2*d***). If the trajectory is in a chaotic zone of the flow (most of the cross section in the case shown—**Figure 2*cii***) (6), then the series formed of its locations in a sequence of transverse cross sections $[x(n\Delta z), y(n\Delta z); n = 0, 1, 2, \ldots]$ explores the entire chaotic zone to which the trajectory belongs; this collection of positions is called a Poincaré map (**Figure 2*ciii***). The tendency for a randomly chosen trajectory to visit an arbitrarily small neighborhood of any point in the chaotic zone as time goes to infinity is called ergodicity in analogy to the tendency of thermodynamic systems to explore their phase space (7). This behavior contrasts that in a nonchaotic flow for which the positions will be confined to a single streamline (**Figure 2*diii***). This distinction in the manner in which trajectories explore the domain of a flow has particular consequences for dispersion and sampling processes.

CHAOS AND TRANSPORT PROCESSES

Aref (8), Ottino (9), Wiggins & Ottino (10), and others (11, 12) have laid the theoretical foundation of chaotic flows. The primary emphasis of many of those studies is the machinery for treating the kinematics of chaotic flows with weak or no molecular diffusion. In this review, we focus on contexts in which molecular diffusion cannot be neglected and thus plays an important role in defining the impact of chaotic dynamics on transport. We provide the minimal review of the mathematical foundation of chaotic flow required to treat convective-diffusive processes. We attempt instead to provide physical explanations and simple mathematical tools as well as to map onto concepts that are familiar from standard courses on transport phenomena (13). Whenever possible and appropriate, we emphasize the ways in which chaotic flows change rates of transfer qualitatively or quantitatively relative to those found in similar nonchaotic flows.

We focus on four transport processes (**Figure 1**): (*a*) mixing, the homogenization of miscible components of a fluid under the parallel action of convection and diffusion (**Figure 1*a***); (*b*) interfacial transfer of heat or solute from a fluid to an interface with a solid, an immiscible fluid, or a domain in the fluid that is convectively separated (**Figure 1*b***); (*c*) dispersion or spreading of heat or mass in a mean flow (**Figure 1*c***); and (*d*) spatial sampling, a less familiar process motivated by massively parallel biological binding assays (so-called "biochips") in which a diverse ensemble of solutes must explore a similarly diverse ensemble of binding sites presented on a solid substrate (**Figure 1*d***). In each subsection, we present specific applications and challenges with the discussion of experimental, theoretical, and computational approaches. We emphasize Newtonian fluids, microfluidic systems (an active context in the past decade for applications and

basic studies), and mass transfer relative to heat transfer; when possible, we point to the relevance of our discussion beyond this scope.

Modeling Convection-Diffusion Processes

For a single-phase system, the evolution of a scalar field (energy or solute—we will proceed with solute transport) owing to fluid flow is described by the convection-diffusion equation in the laboratory or Eulerian frame,

$$\frac{\partial c}{\partial t} = D\nabla^2 c - \mathbf{u}\cdot\nabla c, \qquad 1.$$

where $c(x, y, z, t)$ is the concentration of the solute, $\mathbf{u}(x, y, z, t)$ is the velocity field, and D is the diffusivity (13). For the purposes of this review, we assume that $\mathbf{u}$ is known and consider scenarios in which solute fluxes do not influence the flow; this scenario corresponds to the limit of weak concentration gradients. Despite the apparent simplicity of Equation 1 with these restrictions, it typically does not yield analytical solutions owing to the possible complexity of the convection term (second term on the right) and boundary conditions. Many important transport processes involve homogeneous or heterogeneous reactions. We do not consider homogeneous reactions explicitly, and when we consider heterogeneous reactions, we take them to be fast such that they impose a concentration boundary condition, $C(\text{boundary}) = 0$. To account for the importance of convection relative to diffusion, we define the Péclet number, $Pe \equiv UH/\mathrm{D} = (H^2/D)/(H/u)$, where u and H are the characteristic velocity and dimension of the flow. We can interpret Pe physically as the ratio of the diffusion time to the convection time across the characteristic dimension of the system.

In considering transport in chaotic flows, it is instructive to rewrite Equation 1 in the frame of reference of diffusive tracers evolving in the flow, the Lagrangian frame,

$$\frac{\mathrm{d}\mathbf{x}_i}{\mathrm{d}t} = \mathbf{u} + \mathbf{B}(t), \qquad 2.$$

where $\mathbf{x}_i = x_i\hat{x} + y_i\hat{y} + z_i\hat{z}$ is the instantaneous position of the ith tracer and $\mathbf{B}$ is the stochastic contribution to the velocity owing to Brownian motion. Equation 2 governs the trajectories of individual tracers. It is these trajectories that can display chaotic behavior, even in the absence of diffusion ($\mathbf{B} = 0$) and for a velocity field (**Figure 2*ci***) that is perfectly regular in the Eulerian frame (3). For this reason, chaotic fluid motion is often called Lagrangian chaos. One common means to study the dynamics of diffusive and nondiffusive particles in chaotic flows is to numerically integrate Equation 2 forward in time for tracers launched from various initial positions. A central challenge of theoretical approaches is the prediction of the structure of these trajectories and the rates of transport processes that they define with a minimum amount of Lagrangian information derived from such simulations.

Achieving Chaotic Flow

Before considering convection coupled to diffusion, we provide a brief, practical guide for the design of laminar flows that display chaos. Ideally, this guide would provide strict criteria in terms of the Eulerian characteristics of the flow (for example, geometry and typical strain rates) that would guarantee chaos and allow for the maximization of the volume of the chaotic regions within the flow. Unfortunately, such rules have not been elucidated, and one must use numerical simulation of trajectories (via Equation 2) or experimental measurements within a given flow to test for exponential stretching and identify chaotic zones (for example, with Poincaré mapping;

see **Figure 2*ciii***). Fortunately, however, some general rules and guidelines do exist. A necessary but insufficient criterion for the existence of chaos is that the flow must be 2D (two nonzero velocity components) and time dependent or 3D (three nonzero velocity components). Such flows typically contain chaotic zones, although the fraction of the domain occupied by these zones may be infinitesimal. A rule of thumb that can aid in the design of large chaotic domains is as follows (**Figure 2*ci*** illustrates the case of a steady 3D flow): vary the velocity field along the mean flow (**Figure 2*ci***, *left*, *middle*) or in time such that the instantaneous streamlines, when superimposed (**Figure 2*ci*, *right***), are transverse to each other over as much of the domain as possible. Roughly speaking, the more orthogonal the streamlines are ($\phi \rightarrow 90°$) at a given point, the stronger the tendency for chaos is around that point. Sturman & Wiggins (14) have attempted to formalize this argument and have shown with numerical simulation that reasonable predictions can be achieved. Experimentally, steady 3D flows are achieved with spatial variation in the geometry (15, 16), and time-dependent 2D flows are achieved with the application of pulsatile pressure gradients (17) or electric fields (18). Instabilities owing to inertia [for example, Dean vortices (19, 20)], viscoelasticity (21, 22), or electrohydrodynamic effects (23, 24) also produce appropriate time dependence and 3D structure.

MIXING

We define mixing as a process by which miscible fluids are homogenized to a molecular scale via diffusion alone or via diffusion operating in parallel with convection, as captured by Equations 1 and 2. Mixing in simple liquids plays an important role in the initiation of chemical reactions and in the maintenance of homogeneity within reactors. In these contexts, the time to mix (homogenize) must be short compared with that of the chemical reaction or the residence time of the reactor (for example, in continuous-feed stirred tank reactors) (25, 26). An appropriate flow for mixing should deform the fluid such that the length scale over which heterogeneity exists [$s(t)$ in **Figures 1*a*** and **2*a*,*b***] decreases rapidly in time or with position along a mean flow. Clearly, the promise of exponential thinning [for example, $s(t) = s_0 \exp(-\gamma t)$, where γ is the strain rate] makes chaotic flow an attractive option.

Chaotic Laminar Mixers

Strategies for generating exponential stretching in laminar mixers predate the formal identification of chaotic flows. For example, the use of impellers on an orbiting rotor (familiar from classic Kitchen Aid® mixers) (27) produces a time-dependent, quasi-2D flow that mixes efficiently. Polymer extruders (28) and static mixers such as the Kenics® design (29) can achieve a close approximation of the extensional baker's transformation (**Figure 2*a***). In these cases, varying the shape of the cross section of a conduit generates secondary flows that stretch, cut, and reassemble the fluid as it moves in the mean flow.

Interest over the past two decades in the scale-down of chemical process for lab-on-a-chip applications (30) has motivated the development of mixers that can be fabricated and operated on submillimeter dimensions, which are known as micromixers. For processing single-phase flows, micromixers have been demonstrated that borrow design strategies from macroscopic static mixers to perform a baker's transformation on the fluid (16). **Figure 3*a*** presents one such split and recombine (SAR) design (16). The micrographs in **Figure 3*aii*** indicate an exponential increase in the number (two, four, eight . . .) of striations of the two solutions and an exponential decrease in their thickness. Advantages of SAR designs include a relatively uniform rate of deformation (leading to uniform striation thicknesses) and a compact design because the strain rate in secondary

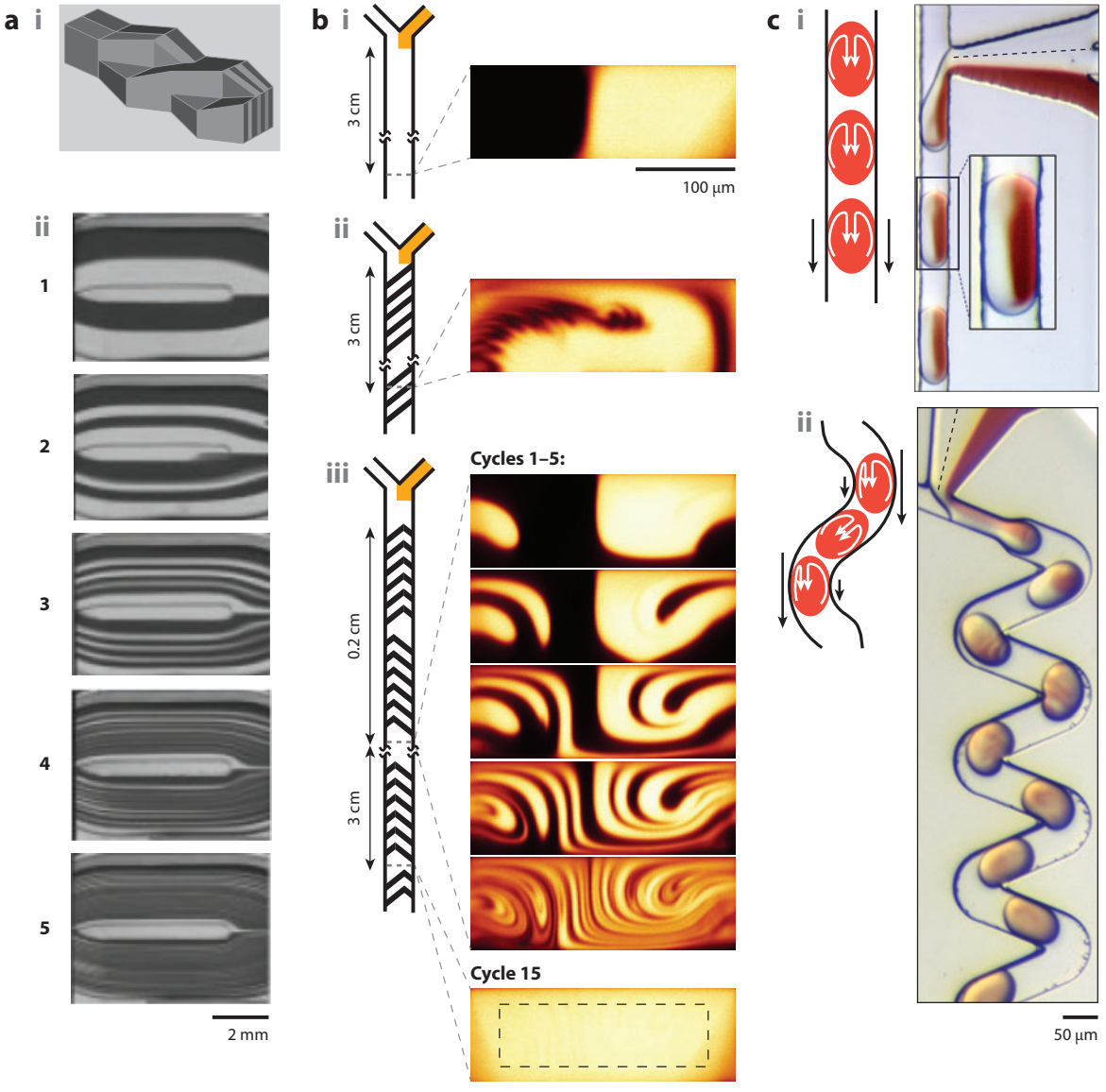

Figure 3

Examples of laminar mixing. Mixing is visualized using a solution of dye and a pure solvent. (*a*) Split and recombine (SAR) mixer. (*i*) The geometry of an SAR mixer is shown. (*ii*) Optical micrographs show the concentration profiles at the end of cycles one to five in the SAR mixer at *Re* 0.22 and $Pe \sim 10^6$. Adapted from Schönfeld et al. (16) with permission of The Royal Society of Chemistry. (*b*) Nonchaotic and chaotic mixing in microchannels with grooves. Confocal fluorescence micrographs show the evolution of a stream of solution of fluorescent dye undergoing pressure-driven flow in the cross section of microchannels. (*i*) Channels with no grooves mix by diffusion alone. (*ii*) The addition of grooves on one wall of the channel in a uniform pattern generates a vortical secondary flow that is nonchaotic. (*iii*) A variable pattern of grooves in the form of staggered herringbones leads to a chaotic secondary flow. Schematic diagrams indicate the pattern of grooves on the floor of the channel. Reprinted from Stroock et al. (15) with permission from AAAS. (*c*) Mixing in multiphase flows. Optical micrographs show droplets with an inhomogeneous distribution of solute injected into an immiscible continuous phase. Schematic diagrams show the streamlines inside the droplets. (*i*) Steady recirculation occurs in droplets as they propagate along a straight channel. Adapted with permission from Tice et al. (32). Copyright © 2003 American Chemical Society. (*ii*) Unsteady, chaotic recirculation occurs in droplets as they propagate through a serpentine channel. Adapted from Bringer et al. (34).

flow is of the same order as the strain rate in mean flow. The principal disadvantage of SAR mixers is that the complexity of their architecture complicates fabrication and could lead to fouling.

Figure 3*b* presents an alternative design for a static micromixer based on the inclusion of diagonally oriented grooves on one wall of a microchannel (**Figure 3*bii*,*iii***); these grooves generate transverse secondary flows (15, 31). The trajectories presented in **Figure 2*c*,*d*** were generated from a model of the flows in channels such as in **Figure 3*bii*,*iii***. This design is easily generated on submillimeter dimensions by standard microfabrication techniques, but it generates weaker deformations than SAR designs and thus requires longer mixing lengths. This example illustrates the qualitative differences in the rate of mixing achieved without secondary flow (**Figure 3*bi***) and with nonchaotic (**Figure 3*bii***) and chaotic secondary flows (**Figure 3*biii***): at a distance of 3 cm down the channel at high *Pe* ($Pe \sim 10^6$), negligible transverse mixing has occurred in the absence of secondary flow (**Figure 3*bi***), dispersal without significant homogenization has occurred with an unchanging secondary flow (**Figure 3*bii***), and substantial homogenization has occurred with a variable secondary flow (**Figure 3*biii***).

Figure 3*c* presents a study of mixing in a liquid-liquid multiphase flow in a microfluidic channel (32–34). A train of droplets containing segregated aqueous solutions was injected into an immiscible carrier fluid. As has been long appreciated (35), the relative motion of two fluid phases generates secondary flows in both the continuous and dispersed phases, as shown schematically in **Figure 3*ci*** (inner flow shown). As indicated in the micrograph, this steady, quasi-2D flow does not induce efficient mixing. **Figure 3*cii*** shows that the introduction of simple curves in the path of the channel achieves the time dependence that is required for chaos; the micrograph indicates that rapid mixing was achieved. For similar strain rates, chaotic flows induce mixing that is qualitatively faster than that of nonchaotic flows.

The Ranz Stretch Model of Mixing

We now turn to a discussion of models of mixing. To develop a simple model of laminar mixing that captures both chaotic and nonchaotic flows, we return to the baker's transformations presented in **Figure 2*a*,*b***. Ranz (5) proposed an insightful, approximate approach in which these linear flows (pure extension and simple shear) are associated with the local experience of fluid elements in real flows (chaotic and nonchaotic, respectively). To implement this local perspective in the context of mixing, he considered convection-diffusion in a Lagrangian reference frame, (x', y'), that follows the position and orientation of a striation within the evolving mixture (inset in **Figure 4*a***; see also **Figure 1*a***). In this frame, he proposed a stretch model in which the convection diffusion equation

Figure 4

Characterization of mixing. (*a*) Predictions of the Ranz model for baker's transformations. (*i*) The evolution of the concentration in steady linear flows obeys Equation 5 in ξ-τ space such that the standard deviation (SD) is predicted to follow a universal decay with τ for all values of *Pe* [$= \gamma s(0)^2/D$] and initial distributions [$s(0)$ and $\lambda(0)$]. (*ii*) When plotted relative to axial position [assuming a superimposed axial plug flow with axial position $= 10\ \gamma s(0)t$, with strain rate, γ; real time, t; and the prefactor matching the ratio of axial to transverse flow in panel *b*], the Ranz model predicted dramatically faster decay of SD in extensional flow relative to simple shear flow or pure diffusion. (*b*) Experimental measurements of SD in chaotic, nonchaotic, and uniaxial Poiseuille flows show qualitative similarity to the predictions in subpanel *aii* if the *Pe* numbers are matched. Reprinted from Stroock et al. (15) with permission from AAAS. The experimental data are plotted versus axial position in the duct. (*c*) Logarithmic scaling of time to achieve 90% homogeneity (SD $= 0.1$) with *Pe* number for different solutes and geometries is seen for mixing in droplets. Adapted from Bringer et al. (34). (*d*) Evolution of the concentration probability distribution $p(c)$ in the chaotic flow shown in the inset at late times and its prediction using the random merging model. (The prefactor N is the number of pixels sampled in each image in the inset.) Adapted from Villermaux et al. (37).

(Equation 1) reduces to

$$\frac{\partial c}{\partial t} - \alpha x' \frac{\partial c}{\partial x'} = D \frac{\partial^2 c}{\partial x'^2}, \qquad 3.$$

where $\alpha = -\mathrm{dln}[s(t)]/\mathrm{d}t$ is an effective rate of extension along y', $s(t)$ is the width of the strands at time t, and D is the molecular diffusivity of the solute of interest. In Equation 3, we neglect diffusion along the extensional direction at a high Péclet number [$Pe = \gamma s(0)^2/D$, where $s(0)$ is the initial length scale of segregation in the mixture and γ is the strain rate in the flow]. The rate, α, represents the instantaneous extensional component of the local, linear flow experienced along the orientation of the striation, y'. For evolution in pure extension, $\alpha = \gamma$, and for simple shear,

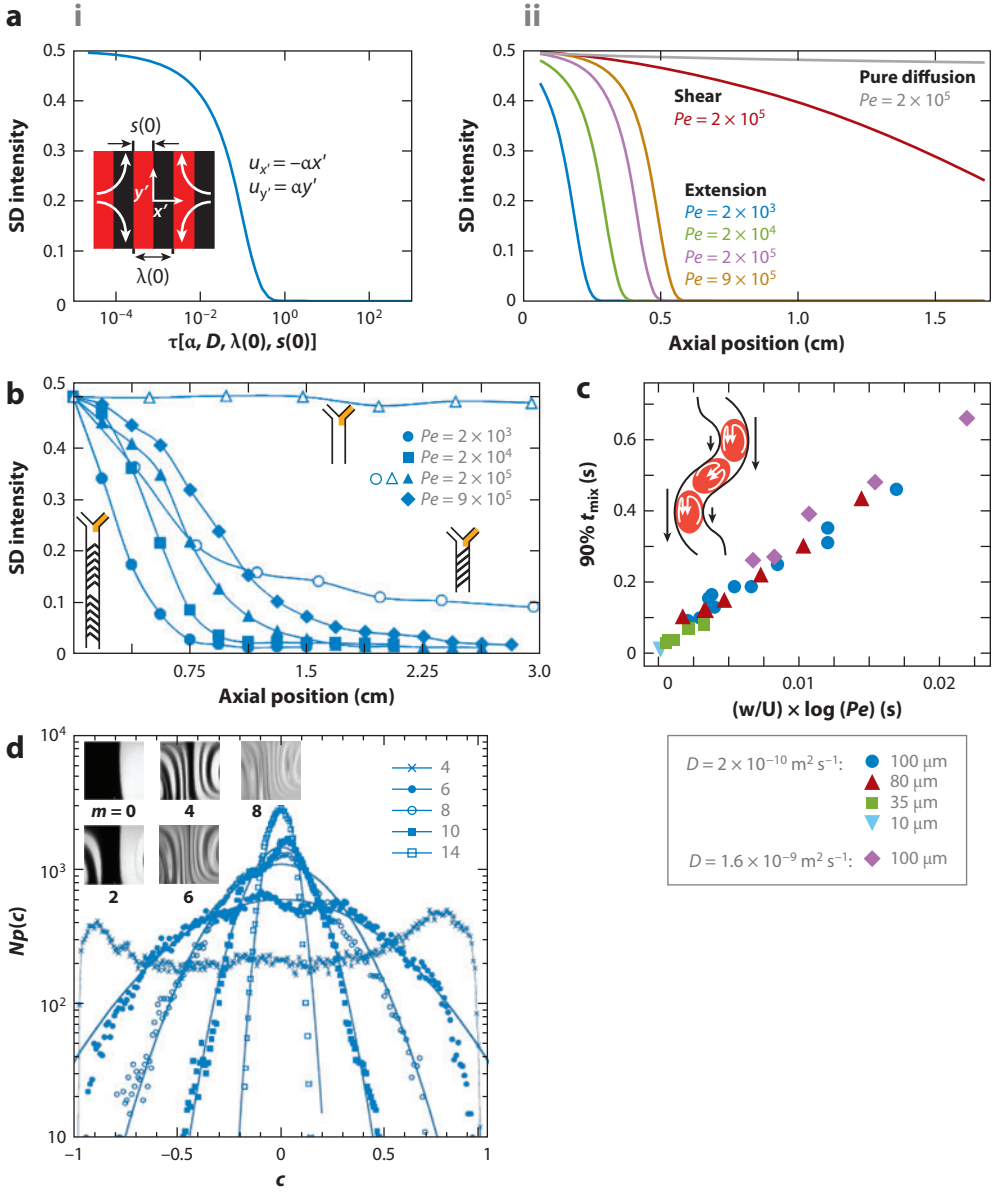

$\alpha = (\gamma t)/\{[1+(\gamma t)^2]\}$. If we take a periodic array of striations (infinite in y') as the initial condition, $c(x', y', t = 0)$, the stretch model provides an exact treatment of mixing in the extension and shear versions of the baker's transformations (**Figure 2*a,b***).

Ranz (5) further introduced the following change of variables:

$$\xi = \frac{x'}{s(t)} \quad \text{and} \quad \tau = \int_0^t \frac{D}{s(t')^2} dt', \qquad 4.$$

with which Equation 3 reduces to

$$\frac{\partial c}{\partial \tau} = \frac{\partial^2 c}{\partial \xi^2}. \qquad 5.$$

The evolution in ξ-τ space thus proceeds as pure diffusion with a nondimensional diffusivity of one. The convective-diffusive time, τ, represents the time required for a distribution of solute undergoing pure diffusion to achieve the same degree of homogeneity as the distribution would in the flow under consideration after a dimensional time, t. Equation 5 indicates a unity of mixing dynamics in linear flows. Indeed, if we track the progression of mixing as the standard deviation (SD) of the concentration field as predicted by Equation 5, we find the universal curve in τ-space (**Figure 4*ai***). We see that τ encodes the progress of mixing in a given flow; substantial mixing will have occurred for $\tau = O(1)$. Evaluating τ in Equation 4 gives expressions for the convective-diffusive time for pure extension, simple shear, and no flow:

$$\tau_{ext} = \frac{D[\exp(2\gamma t) - 1]}{2\gamma s(0)^2}, \tau_{shear} = D\frac{t + \gamma^2 t^3/3}{s(0)^2}, \quad \text{and} \quad \tau_{diff} = \frac{Dt}{s(0)^2}. \qquad 6.$$

These expressions predict that extension leads to qualitatively different scaling of the mixing time than does simple shear. For large Pe, $t_{ext}(\tau = 1) = (1/2\gamma)\ln[2\gamma s(0)^2/D] = (1/2\gamma)\ln(2Pe)$ and $t_{shear}(\tau = 1) = (1/2\gamma)\,(12Pe)^{1/3}$; the exponential stretching in the flow leads to logarithmic rather than power law dependence on Pe [Rhines & Young (36) showed that this scaling ($Pe^{1/3}$) typically holds only for a short time and is followed by linear scaling in Pe]. In **Figure 4*aii***, we use Equation 6 to replot the decay of SD with respect to real time for extension (at various values of Pe), simple shear, and pure diffusion. As expected, extension leads to qualitatively faster mixing than the other cases and weak dependence on Pe.

Quantitative Measurements of Mixing and Extended Theories

We turn to measurements of mixing in real flows and ask whether the predictions of the stretch model, with its focus on the local linear flows, are relevant. **Figure 4*b*** presents the decay of SD of concentration from the experiments presented in **Figure 3*b*** in groove-based micromixers. The values of Pe match those used in the stretch model in **Figure 4*aii***. We note qualitative agreement between the simple model and the experiment. In particular, the weak variation of the mixing time with Pe predicted by the stretch model for pure extension is observed for the chaotic flow. **Figure 4*c*** presents the variation of mixing time (defined as the time for the SD of concentration to decay to 10% of its initial value) with Pe for droplet-based mixing in serpentine channels (**Figure 3*cii***). For various channel geometries we see robust scaling of mixing time with $\log(Pe)$, as predicted. We conclude that Ranz' approach captures the basic physics of mixing in real flows. In particular, the rapid mixing achieved in chaotic flows can be attributed to the persistent extension that they impose on the fluid, as in the extensional baker's transformation.

Clearly, the stretch model is an oversimplification that fails to capture the finer details of the evolution of the concentration during mixing in realistic flows. Importantly, real flows contain a distribution of strain rates. The distribution of striation widths seen in **Figure 3*biii*** arises from

the experience of different strain histories in different parts of the flow. This distribution in turn leads to the more gradual decay of SD that is observed for the chaotic cases in **Figure 4*b*** relative to the predictions in **Figure 4*aii***. This same effect of multiple rates impacts the late stages of mixing when striations with distinct strain histories merge. Villermaux et al. (37) have proposed a model for this process that treats the merging via a self-convolution of the histogram of concentrations, $p(c)$. **Figure 4*d*** illustrates that his model successfully captures the form and evolution of $p(c)$ for the chaotic version of the groove-based mixer. The stretch model also neglects the influence of boundaries on the flow. In a theoretical treatment of chaotic mixing in bounded domains, Chertkov & Lebedev (38) and Lebedev & Turitsyn (39) predict that near-wall regions will dominate the late-time evolution of the concentration distribution and that the mixing time should scale as $Pe^{1/4}$ rather than as $\log(Pe)$. The Groisman group provided a convincing experimental validation of this scaling with a static micromixer (40). In our judgment, consensus has yet to be reached on a general theory (valid for all times and Pe) of mixing in chaotic flows. Furthermore, the presence of both chaotic and nonchaotic regions in many practically achievable flows poses a challenge (11); the predictions of scaling discussed above fail to account for such composite structure, although one expects that the rate of diffusive exchange between these regions in the flow will dominate late stages of mixing. We maintain, nonetheless, that Ranz's stretch model provides a valuable conceptual basis and a useful tool for first-order analysis of mixing processes.

INTERFACIAL TRANSFER FROM CHAOTIC FLOWS

Interfacial transfer refers to the motion of heat or solute to or across an interface between two fluids or between a fluid and a solid. This transfer is essential to the success of many processes that operate under laminar flow conditions in both macro- and microscale systems, such as heat exchanger design (41–44), electrochemical systems for analysis and energy production (45, 46), separations with membranes (47) and without membranes (48), and sensors involving interfacial reactions (49–53). In considering the impact of the character—chaotic or nonchaotic—of a flow on interfacial transfer, it is tempting to view the process as a special case of mixing in which the scalar is continuously injected into the bulk of the flow. With this view, which implicitly assumes that homogenization in the bulk is the rate-limiting step, one might expect that chaotic flows could, in general, provide qualitatively faster rates of transfer than nonchaotic flows. As the following illustrates, chaos can indeed modify rates of interfacial transfer but in a manner that is subtler than that for direct mixing processes.

Examples of Interfacial Mass Transfer from Chaotic Flows

Figure 5 presents two experimental contexts in which interfacial transfer has been measured for comparable chaotic and nonchaotic flows. The diagrams in **Figure 5*a*** show platforms for the extraction of a solute (a fluorescent dye) from a dispersed aqueous phase into a continuous organic phase. A train of droplets was injected into the continuous phase and passed through either a straight (**Figure 5*ai***) or serpentine (**Figure 5*aii***) channel to generate either nonchaotic or chaotic flow within the droplets (54), as in the experiments presented in **Figure 3*c***. The pattern of fluorescence intensity within the droplets suggests a symmetric, steady flow in the droplets for the case of the straight channel (**Figure 5*ai***) and irregular flow within the droplet for the case of the serpentine channel (**Figure 5*aii***). Mary et al. (54) quantified the rates of extraction in the two flows and found that, surprisingly, the magnitudes and time evolution of the rates were quantitatively similar at a given Pe.

Figure 5*b* presents an example of mass transfer to a liquid-solid interface in an electrochemical cell. In this potential cell (55), the counter electrode (microchannel floor) could be flat (uniaxial flow), covered with a uniform pattern of grooves (nonchaotic 3D flow), or covered with a varying pattern of herringbone-shaped grooves (chaotic 3D flow), as in the mixers presented in **Figure 3*b***. With a reversible redox species (ferricyanide/ferrocyanide) in the flowing electrolyte, an applied potential generated a measured electrical current that was limited by the rate of mass transfer to the flat working electrode (56). The Sherwood number (*Sh*) is the nondimensionalized mass transfer coefficient, $Sh(z) \equiv Hk(z)/D$, where H is the height of the channel, k is the local mass

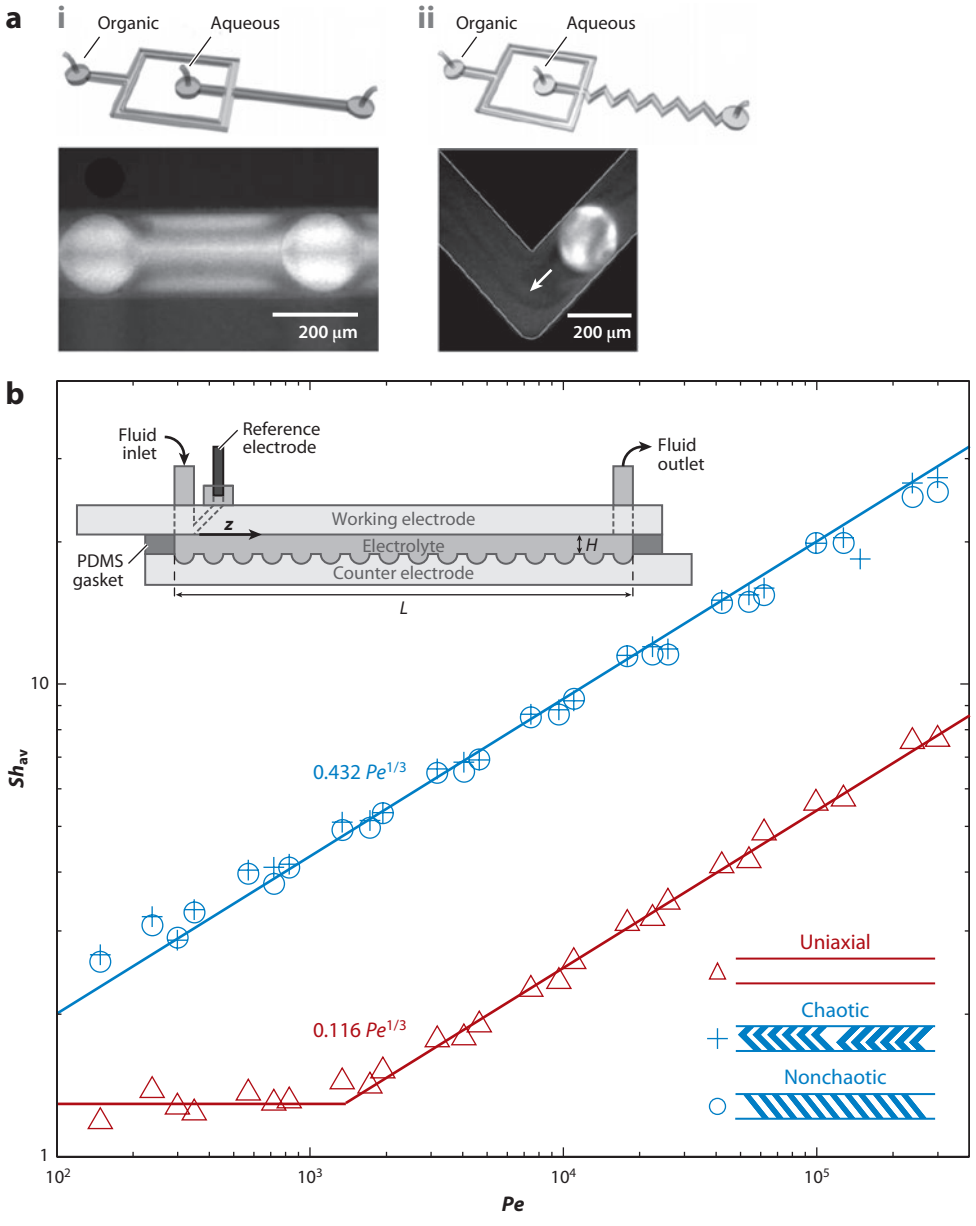

transfer coefficient, and D is the molecular diffusivity of the redox species. The average Sherwood number was calculated from the measured current, I, as follows:

$$Sh_{av} = \int_0^L Sh(z)\mathrm{d}z = \frac{1}{D}\frac{H}{WL}\frac{I}{FC_0}, \qquad 7.$$

where H, W, and L are the height, width, and length of the channel; F is Faraday's constant; and C_0 is the concentration of redox species at the inlet. **Figure 5*b*** presents $Sh_{av}(Pe)$ for the three types of counter electrodes. In all cases, Sh_{av} follows robust power laws at high Pe: $Sh_{av} \sim Pe^{1/3}$; this scaling matches that from the classic analysis of Grætz for uniaxial pipe flows, as presented in standard texts on transport phenomena (13). Also, the presence of the secondary flows over grooves significantly increased the mass transfer rates (~threefold). Finally, as observed for the liquid-liquid extraction, the measured rates were nearly identical for the chaotic and nonchaotic flows. These observations indicate that the presence of secondary flows can lead to significantly higher rates of interfacial transfer relative to comparable uniaxial flows, but that the presence of chaotic flow in the bulk does not have a significant impact relative to nonchaotic flow. Similar conclusions were reached in heat transfer experiments through straight and coiled pipes (44). We attempt to explain these observations below.

Analysis of Interfacial Transfer from Chaotic Flows

To gain insight into the mechanisms by which chaotic and nonchaotic laminar flows influence interfacial transfer, we turn to **Figure 6** for the predictions of a numerical simulation of a liquid-solid transfer process such as in the electrochemical experiments in **Figure 5*b***. In these simulations, diffusive tracers were propagated (according to Equation 2) in a model flow that captures the structure of the axial and secondary flows in a channel with grooves on one wall (6); to capture the diffusion-limited reaction, tracers were eliminated upon collision with the top boundary (57). In the uniaxial case (**Figure 6*ai***), a depleted zone grows to occupy the full thickness of the channel before reaching an asymptotic state beyond an entrance length, $z_{ent} \sim 640H$ [$\sim 0.1PeH$, as in the Grætz problem (13)]. In contrast, for a chaotic secondary flow (**Figure 6*aii***), a thin depleted zone is rapidly established with a thickness that remains constant beyond a short entrance length, $z_{ent} \sim 80H$ ($\ll 0.1PeH$). For the nonchaotic secondary flow (**Figure 6*aiii***), again a thin depleted zone rapidly forms, followed eventually by growth to the full thickness of the channel as the depleted fluid is convected all the way around the cross section. In

Figure 5

Interfacial mass transfer from stirred laminar flows. (*a*) Interphase mass transfer from droplets in microfluidic flows. Schematic diagrams show microfluidic devices for liquid-liquid extraction with (*i*) nonchaotic and (*ii*) chaotic flows within droplets. The fluorescence images show droplets traveling through straight (nonchaotic, subpanel *i*) and serpentine (chaotic, subpanel *ii*) channels with transfer of a fluorescent dye from the droplet into the continuous phase. Adapted with permission from Mary et al. (54). Copyright © 2008 American Chemical Society. (*b*) Electrochemical measurements of rates of mass transfer in microfluidic potential cells. (*Inset*) A schematic diagram of a potential cell. The top and bottom walls of the channel acted as working and counter electrodes, respectively. A gasket made of PDMS (polydimethylsiloxane) forms the side walls, defining a channel with height H and length L. The grooves of the mixing structure (as in **Figure 3*b***) were on the counter electrode (*bottom*). Globally averaged Sherwood numbers (Sh) evaluated via Equation 7 from measured current are plotted versus Péclet number (Pe) for uniaxial flow over a smooth counter electrode (*triangles*), 3D, chaotic flow over a counter electrode with staggered herringbone motif (*crosses*), and 3D, nonchaotic flow over a counter electrode with a uniform pattern of oblique grooves (*circles*). Experiments were run with the reversible redox species ferricyanide/ferrocyanide. Adapted from Kirtland & Stroock (56).

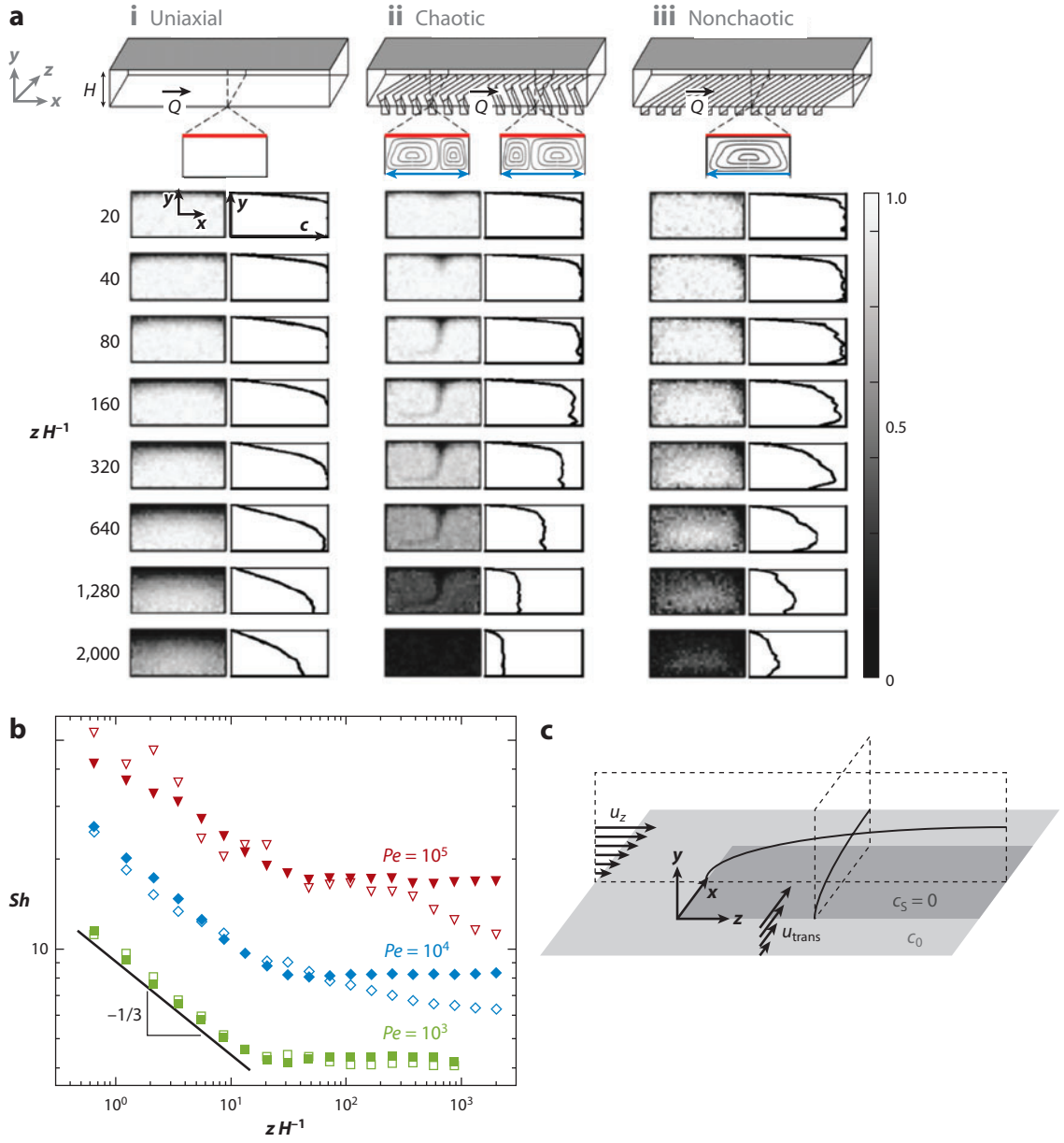

Figure 6

Modeling interfacial mass transfer. (*a*) Simulation of mass transfer to a reactive boundary with diffusive tracers in a duct of height *H*. Schematic diagrams present the cases modeled: (*i*) uniaxial duct flow, (*ii*) chaotic 3D duct flow such as is generated over grooves in the form of staggered herringbones, and (*iii*) nonchaotic 3D duct flow such as is generated by a uniform pattern of oblique grooves. In all cases a fast reaction occurs on the top boundary. Snapshots of concentration are shown for the three cases at various axial positions (*z/H*). (*b*) Evolution of local Sherwood numbers (*Sh*) along the length of the channel for the chaotic flows in subpanel *aii* (*filled symbols*) and for the nonchaotic flows in subpanel *aiii* (*open symbols*) at three values of Péclet number (*Pe*). (*c*) Schematic diagram showing competing boundary layers in the axial and transverse directions that develop because of surface reaction in a transversely stirred laminar flow. u_z and u_{trans} are represented as shear flows in the axial and transverse directions, and the region $c_s = 0$ (*dark gray*) represents the reactive surface. Reprinted with permission from Kirtland et al. (57). Copyright © 2006 American Institute of Physics.

Figure 6*b*, this evolution can be seen quantitatively in the local Sherwood number, $Sh(z)$: for the chaotic case and the nonchaotic case, $Sh(z)$ initially decays as $z^{-1/3}$, as in the Grætz problem $\{Sh(z) \sim [z/(PeH)]^{-1/3}\}$ (13). Unlike the classic result, however, the entrance length is independent of Pe ($z_{ent} \sim PeH$ in Grætz). Beyond this short entrance region, $Sh(z)$ plateaus to a Pe-dependent asymptotic value, $Sh_{asy} \sim Pe^{1/3}$, again unlike the Grætz problems, for which $Sh_{asy} = O(1)$. Finally, at large axial distance, the behavior in the chaotic and nonchaotic flows differs in a subtle way: in the chaotic case, $Sh(z)$ remains constant, whereas in the nonchaotic case it eventually decays. The chaotic flow maintains this asymptotic state by homogenizing the depleted solution in the bulk before it can return to the reactive boundary (**Figure 6*aii***). In contrast, the nonchaotic flow fails to homogenize the depleted solution before it returns to the boundary (**Figure 6*aiii***).

These observations aid in the understanding of the experimental measurements discussed in the previous subsection (**Figure 5**): secondary flows arrest the growth of the depletion boundary layer by convecting the depleted solution off of the reactive boundary. In this manner, stirring in the bulk maintains higher rates of interfacial transfer by maintaining higher gradients than in a uniaxial flow; both chaotic and nonchaotic flows achieve this effect in the early stages of the process. Because the bulk of the transfer occurs in this early stage, we predict that the global rate of transfer (integrated axially) will be relatively insensitive to the eventual decay of $Sh(z)$ for nonchaotic flows; this prediction is compatible with the observation that chaotic and nonchaotic flows provide similar global rates of transfer in processes such as those in **Figure 5**. On one hand, for interfacial transfer processes that involve the decay of an initial difference in temperature or concentration, chaotic flows may provide little added benefit relative to comparable nonchaotic flows. On the other hand, for processes that require steady interfacial transfer, such as for thermal control of an exothermic reaction in a plug flow reactor, the maintenance of a high value of Sh_{asy} is important, and chaotic flows are preferable.

Can we formulate a correlation of the simple evolution of $Sh(z)$ seen in **Figure 6*b*** for transfer from chaotic flows? The conceptual picture of the near-boundary region of a stirred flow in **Figure 6*c*** suggests a simple approach for calculating $Sh(z)$ (57): a principal flow (along z) impinges on the leading edge of the unbounded axis of a reactive interface and a boundary layer begins to grow; simultaneously, a transverse, secondary flow (along x) impinges on the side edge of the bounded axis of the interface. Importantly, for the simple reason that the transverse dimension of the interface is finite, the secondary boundary layer does not grow indefinitely. Rather, its growth is terminated once it has traversed the width, W, in an axial distance $z_{ent} = \beta W$, where $\beta = U_z/U_{trans}$ is the ratio of the speed of the mean flow to the transverse secondary flow. Once this transverse boundary layer has formed, it terminates the growth of the principal boundary layer by sweeping the material off of the interface, as seen in **Figure 6*aii***. Following Lévêque's (58) analysis of the growth of both the axial and the transverse boundary layers, we predict:

$$Sh(z) = \begin{cases} \dfrac{1}{\Gamma\left(\frac{4}{3}\right)}\left(\dfrac{PeH}{9z}\right)^{1/3} & z < \beta W \\ \dfrac{(3/4)^{1/3}}{\Gamma\left(\frac{4}{3}\right)}\left(\dfrac{H}{W\beta}Pe\right)^{1/3} & z > \beta W \end{cases}. \qquad 8.$$

This modified Grætz correlation agrees well with numerical simulations such as in **Figure 6*b*** (57). Furthermore, analogous correlations work well for transfer to stress-free interfaces within and at the boundaries of flows (exponents are 1/2 rather than 1/3) (59).

We conclude by returning to the connection between the character of mixing and interfacial transfer. In particular, why are chaotic flows able to maintain thin boundary layers and high transfer rates? To answer this question, we have considered in detail the fate of an element of fluid that leaves the transfer interface (for example, depleted of solute) and enters the bulk (59).

As argued earlier, to maintain the thin boundary layer, this element should be homogenized with the bulk before returning to the surface downstream in the mean flow. Considering the scenario in **Figure 6**, we showed via scaling analysis and numerical simulation that the characteristic axial distance traveled by a depleted element of solution before returning to the reactive surface, L_{ret}, is $\sim Pe^{2/3}$, whereas the characteristic length required for homogenization, L_{mix}, is $\sim\log(Pe)$ or, as a weak power law, $L_{mix} \sim Pe^{1/6}$. Thus, at high Pe, we expect that $L_{mix} < L_{ret}$. Chaotic flows should homogenize the bulk sufficiently quickly to avoid reattachment of the solution shed from the boundary layer and should maintain high Sh out to arbitrary downstream distance and to arbitrarily high Pe. We found that for comparable nonchaotic flows, this criterion did not hold ($L_{ret} \sim Pe^{2/3}$ and $L_{mix} \sim Pe$). Thus, the efficiency of mixing in chaotic flows impacts interfacial transfer in a subtle but important way.

AXIAL DISPERSION

We take dispersion to mean the spread of material via convection, diffusion, or the combined action of both. Unlike mixing, dispersion does not imply homogenization on a molecular scale. We focus on axial dispersion of miscible solutions in a nonuniform mean flow (for example, Poiseuille), as shown in **Figure 1*c***. Axial dispersion in laminar flows plays an important role in defining the resolution of chromatographic processes (60) and in the conversions achieved in pipe flow reactors (26, 61). Taylor (62) analyzed the phenomenon for the case shown in **Figure 1*c***, a band of solution of a diffusive solute spreading in a uniaxial Poiseuille flow: at short times, for which the solute has not had time to diffuse across the lateral dimension of the conduit (residence times, $t_{res} \ll H^2/D$, where H is the diameter of the pipe or $z \ll PeH$), volumes of solution at different transverse locations are convected at different speeds down the channel; at the wall they do not move, and in the center they move at the maximum velocity. The band disperses such that its axial extent, Δz, is $\sim U_{max}t$. At late times ($t_{res} \gg H^2/D$ or $z \gg PeH$), Taylor showed that diffusive sampling of the cross section and thus of the distribution of axial velocities leads to diffusion-like broadening of the band with an effective axial diffusivity given by

$$D_{eff} = D\frac{Pe^2}{48} = \frac{(U_z H)^2}{48D}, \qquad 9.$$

such that $\Delta z \sim \sqrt{D_{eff}t}$. Importantly, convective-diffusive diffusivity scales inversely with the molecular diffusivity. Physically, the molecular diffusivity defines the rate at which solute samples the distribution of axial velocities; the faster this sampling, the closer the averaged velocity of each solute will be to the mean of the ensemble. Alternatively, we can express Equation 9 in the generic form for the effective diffusivity of a random motion (7): $D_{eff} \sim U_z{}^2 t_{corr}$, where $t_{corr} = H^2/D$ is the characteristic time for the loss of correlation in the axial motion or the characteristic time to mix by pure diffusion across the channel ($t_{corr} = t_{mix}$). Given that the introduction of chaotic secondary flows can dramatically decrease mixing times, we expect that these flows could provide substantially reduced rates of dispersion.

Experimental Measurements of Dispersion in Chaotic Flows

Experimental studies of the impact of chaotic flow on axial dispersion have been pursued in several systems; we focus on cases in which dispersion in the presence of chaos has been compared with that in nonchaotic flows. **Figure 7*a*** presents a qualitative comparison of dispersion (as residence time distribution) at various positions along a uniaxial flow (**Figure 7*ai***) and along a chaotic flow generated by a pattern of staggered herringbone grooves, as in **Figure 3*biii*** (15). The peaks are

significantly narrower and more symmetrical in the chaotic flow. The symmetry suggests that the dispersion process reached the asymptotic state (the Taylor regime) in which complete sampling of the velocity field has been achieved. **Figure 7*b*** presents another study of dispersion in groove-based mixers (63) in which dispersion in a nonchaotic 3D flow (**Figure 7*bi***) was compared with that in a chaotic flow (**Figure 7*bii***). The peak is slightly narrower and higher in the nonchaotic case; this observation runs counter to our expectation that the efficient sampling provided by a chaotic secondary flow should reduce dispersion. In comparing both these cases with an analytical model of dispersion, Cantu-Perez et al. (63) found it necessary to include exchange between a moving and a stagnant volume of fluid, such as would be present in a disconnected region of the flow near a boundary. This requirement suggests that the secondary flows did not provide uniform mixing within the cross section of the mean flow. Castelain and colleagues (43) worked in coiled pipes in which inertial secondary flows led to chaotic or nonchaotic flow, depending on the geometry of the coils. They found that D_{eff} was up to 25% smaller in the chaotic case relative to the nonchaotic case for large Reynolds numbers (>2,500), but they too found it necessary to consider the presence of a stagnant volume of fluid to explain their measurements (42). These few studies suggest that the presence of transverse secondary flows can significantly reduce dispersion relative to that in uniaxial flows. They leave unclear, however, whether chaotic flows provide a particular advantage relative to comparable nonchaotic ones, and they fail to validate the prediction of distinct scaling for D_{eff} in chaotic flows.

Numerical and Theoretical Predictions of Dispersion in Chaotic Flows

Numerical studies can provide insight into these experimental observations and allow for a deeper investigation of the role of chaos in controlling axial dispersion. **Figure 7*c*** presents the predictions of a tracer-based study (64) in a flow that models that in a coiled pipe at a finite Reynolds number. The plot shows the axial position of diffusive tracers after three different time intervals; the inset shows the Poincaré map for the flow. Particles within the large nonchaotic island within the flow travel as a distinct packet relative to the rest of the population. Complete sampling of the mean flow requires tracers to exchange diffusively between the island and the rest of the flow. This phenomenon illustrates how nonuniformity in the mixing process can slow convergence to the Taylor regime and increase the global rate of dispersion by maintaining purely convective separation of subpopulations of tracers. **Figure 7*d*** presents the analysis of late time dispersion in a related flow for which no large islands exist (64), which provides an opportunity to ask how dispersion proceeds in a pure chaotic flow. The simulation finds $D_{\text{eff}} \sim -\log(D)$ (**Figure 7*d***), which seems to confirm our expectation for a flow that provides exponential stretching and $t_{\text{mix}} \sim \log(Pe)$ (see Mixing section). However, Jones & Young (64) provided a more formal theory to treat dispersion in chaotic flow that indicates a distinct origin of scaling. In a development that parallels that of Koch & Brady (65) for dispersion in a random porous medium, they show that exchange between a diffusive boundary layer and the bulk flow should control the dispersion in a chaotic flow bounded by no-slip walls. On the basis of the scaling of this boundary layer, they predicted $D_{\text{eff}} \sim \log(Pe^{1/3}) \sim -\log(D^{1/3})$, and indeed, this exponent is seen in their simulations (slope of $\sim -1/3$ in **Figure 7*d***). They also predict that the scaling of D_{eff} for $t \gg s_0^2/D$ in nonchaotic flows should be the same as Taylor's original result.

We know of no experimental test of these predictions. Such a study would need to be carried out in a flow for which the absence of nonchaotic islands could be verified. Ottino and colleagues (66) have suggested an experimental method for detecting the presence of islands in steady 3D flows.

SPATIAL SAMPLING WITH CHAOS

We take sampling to refer to a process in which an ensemble of distinct tracers in a flow must reach distinct locations in the domain to, for example, react or bind. For passive, diffusive tracers, this problem is a special case of convection-diffusion-reaction with distinct boundary conditions for each distinct tracer. Related problems arise frequently in biology owing to the vast diversity of chemical species (for example, transcription factors) and of specific binding domains (for example,

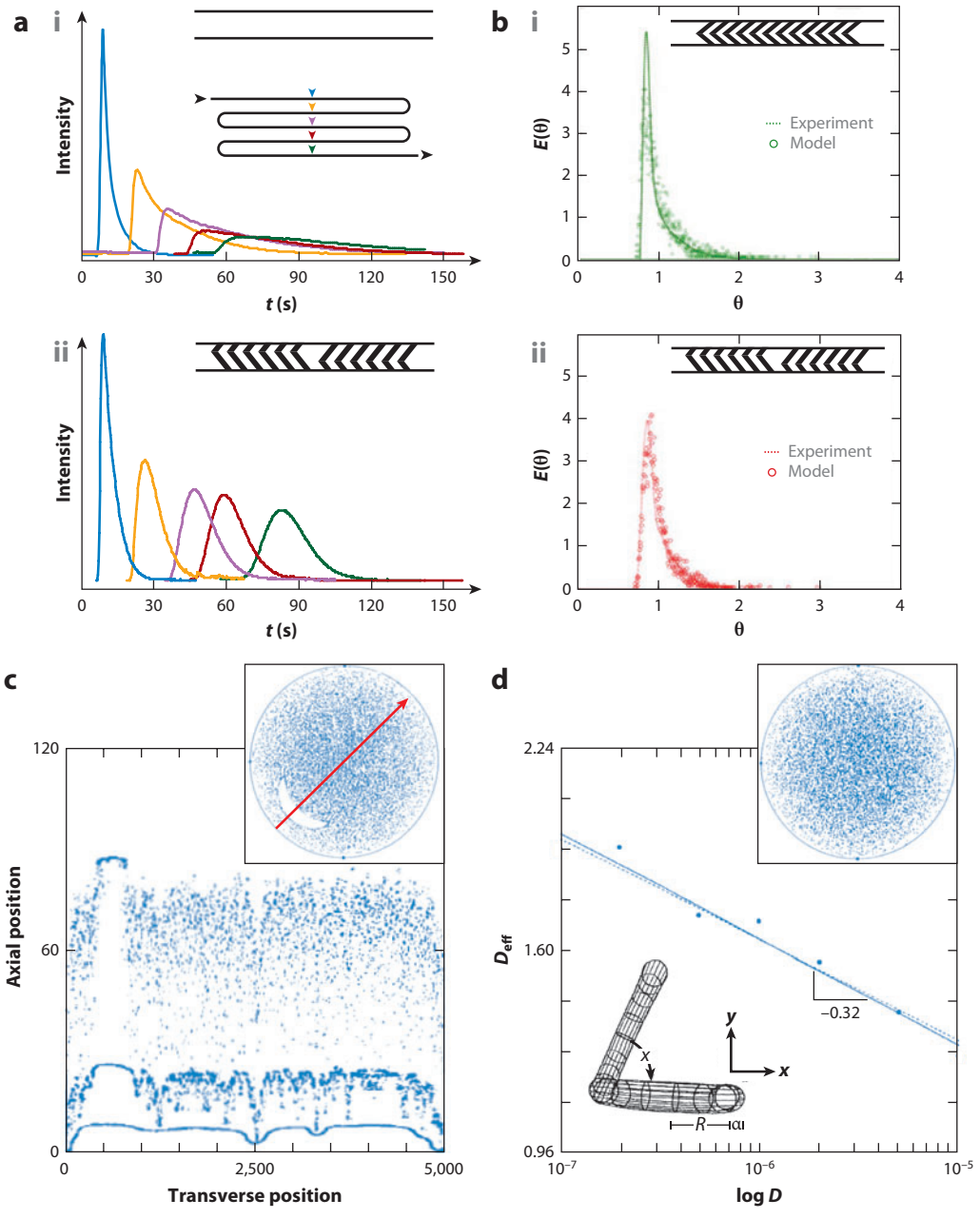

regulatory sequences on genomic DNA) (67). Within living organisms, however, transport often involves active steps that cannot be treated as simple convection-diffusion. Recently emerging biological assays based on biochips have brought this challenge into a technological context. Biochips present a large number (in certain cases, $>10^4$) of distinct DNA- or protein-binding domains in spatially separated regions of a solid substrate (**Figure 1*d***); this substrate is then exposed to a single solution containing a similarly diverse population of binding partners. The presence or absence of specific ligands in the solution is assessed by measuring (typically by fluorescence) the quantity of ligand bound on each region and comparing with a predefined threshold. The mode of delivery of the solution over the substrate should be optimized to maximize the binding rate of each distinct ligand and binding site pair (68). In this context, we might expect that chaotic flows could provide particularly effective sampling on the basis of their ergodicity: any randomly chosen trajectory would eventually come arbitrarily close to every location in the chaotic domain (69).

McQuain et al. (70) introduced this idea and performed a limited test of it in the experiment shown in **Figure 8*a–c*** with a single type of solute (single-stranded DNA) and binding site (complementary single-stranded sequence). **Figure 8*a*** presents a sampling protocol that uses a pulsed source-sink flow for a DNA binding assay: two syringes filled with the DNA solution were connected to four ports into a chamber of large lateral extent (2 cm $\times$ 5 cm) and small height (25 μm); the floor of this chamber presented the binding regions, all of which presented the same complementary DNA strand (70). A repeated flow cycle proceeded in two stages using valves along each branch: (*a*) injection through port A with retraction through port B (**Figure 8*ai***) and (*b*) injection through port C and retraction through port D (**Figure 8*aii***). **Figure 8*b*** presents the streamlines of the flow during the first and second half cycles. In the center of the domain, these streamlines cross one another such that one would expect chaotic trajectories (see subsection on Achieving Chaotic Flow). The total volume, V_{cyc}, of solution passed through the device during a half cycle acted as the control parameter for the flow. The authors chose V_{cyc} to maximize the rate of mixing of a nonbinding dye. **Figure 8*c*** presents a qualitative comparison of the spatial distribution of bound DNA after 4 h of the alternating injection strategy, 4 h of a steady injection process from port A to port B, and 24 h with no flow. The alternating flow clearly produced more uniform binding. In general, the authors found that a stronger signal from bound DNA could be achieved in less time (~fivefold) with the use of an alternating flow pattern.

Hertzsch et al. (69) and Sturman & Wiggins (14) subsequently performed a systematic numerical study of the flows generated by the alternating source-sink strategy in a 2D domain. They emphasized the importance of the structure of chaotic domains within the flow, as seen in Poincaré maps; their study did not consider diffusion. The Poincaré map of a flow generated by a pumping

Figure 7

Axial dispersion in laminar flows. (*a*,*b*) Experimentally measured residence time distribution (RTD) in different flows: evolution of RTD in (*ai*) a uniaxial Poiseuille flow and (*aii*) chaotic flow (using a staggered herringbone motif) at the axial locations indicated by arrows along a 20-cm-long serpentine channel with $Pe \sim 10^4$. Nondimensional RTD in (*bi*) a nonchaotic flow with a symmetrical herringbone motif and (*bii*) a chaotic flow using a staggered herringbone motif at a distance of 22 cm from the inlet at $Pe \sim 10^4$. Panel *a* reprinted from Stroock et al. (15) with permission from AAAS. Panel *b* adapted from Cantu-Perez et al. (63) with permission from Elsevier. (*c*,*d*) Numerical study of axial dispersion in a coiled pipe. In panel *c*, the evolution of a material line in a chaotic flow with islands is shown by the axial variation of particle position in flow with the parameters $Re = 25$, $Pe = 10^{-6}$, and the angle between the curved segments of the pipe $\chi = \pi/2$ (shown schematically in the inset within panel *d*). In panel *d*, the prediction and numerical verification of the logarithmic scaling of the nondimensional effective axial dispersion coefficient with diffusivity. Parameters are $\mathrm{Re} = 62.5$, $\mathrm{Pe} = 10^{-6}$, and $\chi = \pi/2$. The Poincaré maps of the flows used are shown at the top right of panels *c* and *d*. The blank crescent is a large nonchaotic island; the red arrow indicates the approximate transverse axis along which the tracers in the plot were launched. Adapted with permission from Jones & Young (64).

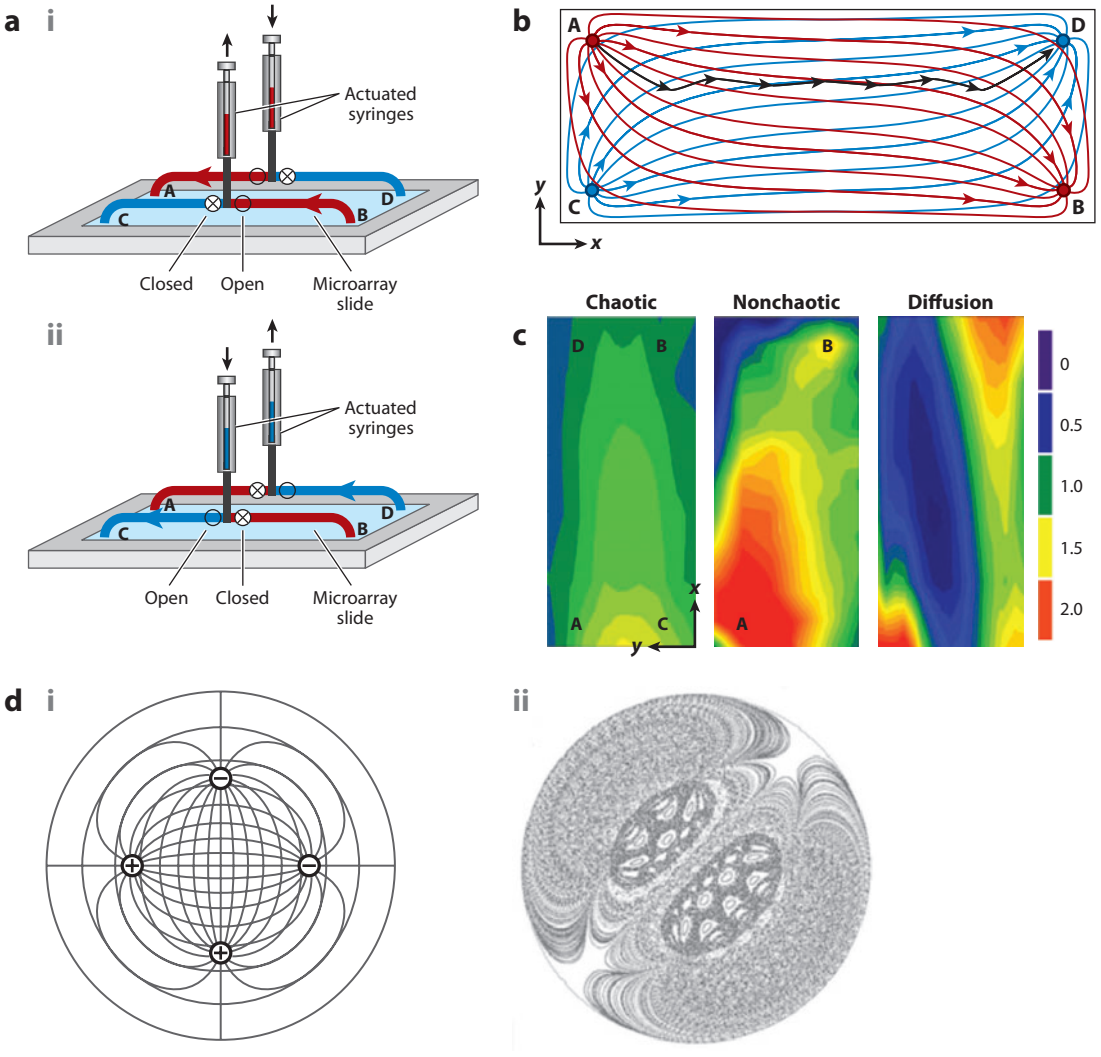

Figure 8

Sampling using chaos. (*a*) A DNA binding assay with chaotic sampling. Schematic diagrams illustrate the generation of a pulsed source-sink chaotic flow using coordinated operation of two pumps and four valves in the two halves (*i*,*ii*) of the pumping cycle. (*b*) Streamline patterns of alternating flows from ports A to B (*red*) and C to D (*blue*). The black line is the path of a particle when red strokes and blue strokes alternate at a pumping rate of 1 μl s^{-1} and a stroke volume of 30 μl. (*c*) Contour plots showing relative spot intensity across the array area for hybridization by chaotic flow, nonchaotic flow, and no flow. Adapted from McQuain et al. (70) with permission from Elsevier. (*d*) Mixing characteristic of the pulsed source sink flow. (*i*) Pumping protocol with sources (+) and sinks (−) similar to the experiment above. (*ii*) Poincaré map of the flow. Adapted from Sturman & Wiggins (14).

strategy similar to that in Sturman & Wiggins (14) shows that chaotic domains interspersed with non-chaotic islands. By varying the position and number of the sources and sinks and V_{cyc}, Hertzsch et al. (69) identified a protocol that eliminated nonchaotic islands on a circular domain. The use of such optimized protocols could lead to improved rates of binding and uniformity. However, the use of Poincaré maps can be misleading in the analysis of rate processes because these maps provide little information on the rate at which a trajectory explores the domain. For example, the

map of the injection protocol that eliminated the islands (69) represents 20,000 cycles of injection, whereas a typical experiment might include a few hundred cycles (70). One cannot know from such a map whether the uniformity that is observed after a long time would be achieved in experimentally relevant times. A complete numerical or theoretical treatment of this sampling problem would also require the consideration of diffusion and interfacial transfer to the binding surface; we are unaware of such treatments at this time. Future experiments with a diverse ensemble of ligands and binding domains should also be pursued.

CONCLUSIONS

We hope that this review convinces the reader that chaotic dynamics can offer a rich and useful element in the design of laminar transport processes. In the most familiar context of mixing, chaotic flows can provide significantly faster homogenization than comparable nonchaotic flows and qualitatively different scaling with *Pe*. With recently proposed designs, the use of chaotic flows has become commonplace in microfluidic systems. Despite significant work on the theory of mixing in chaotic systems, consensus has not been achieved on a general theoretical framework. The impact of chaos on interfacial transfer is subtle, but by allowing for the emergence of an asymptotic state with high Sherwood number ($Sh \gg 1$), chaotic flows could provide significant improvements in the performance of heat exchangers and separation equipment in contexts in which continuous exchange is required. Experimental studies of axial dispersion illustrate the challenges of exploiting the desirable properties of chaotic flows, but models and theory suggest that flows with uniform or nearly uniform chaos could significantly reduce dispersion. In the emerging context of efficient spatial sampling for mediating complicated biochemical assays, experiments suggest the promise of exploiting chaotic dynamics; this theme would benefit from the development of more complete models and extensive experiments. Finally, despite the exotic nature of the underlying dynamics, familiar approaches for modeling convection-diffusion processes can lead to insightful and predictive models for transport in chaotic flows.

Looking forward, some of the experimental and conceptual lessons learned from the interplay of chaos with the transport processes reviewed here can be applied to a broad variety of technological and scientific contexts. A few interesting themes that would benefit from further study are:

1. Reversibility (unstirring) in chaotic flows. Aref & Jones (71) suggested that purification of mixtures of solutes based on stirring and unstirring could take advantage of chaos to increase rates; Tabeling et al. (17) performed one experiment along these lines.
2. Pattern formation in chaotic mixing. Gollub and colleagues (12) demonstrated in a chaotically stirred mixture the emergence of a large-scale spatial structure in parallel with the exponential thinning of fine-scale striations. When coupled to reactions, these complex structures could be used, for example, to pattern features on a substrate.
3. Active migration in complex distributions of concentration. Shraiman and coworkers (72) introduced a generalization of chemotaxis (directed migration of organisms along chemical gradients) to situations in which the organism encounters brief bursts of solute (such as striations in a stirred mixture) rather than steady gradients. This process of infotaxis could play an important role in the dynamics of microorganisms in bioprocessing as well as in the migration of larger organisms in their natural ecosystems.

DISCLOSURE STATEMENT

The authors are not aware of any affiliations, memberships, funding, or financial holdings that might be perceived as affecting the objectivity of this review.

ACKNOWLEDGMENTS

We thank Donald Koch and Joseph Kirtland for helpful discussions. We acknowledge support from the National Science Foundation (CTS-0529042) and the Department of Energy (DE-FG02-05ER46250).

LITERATURE CITED

1. Arnold VI. 1965. Sur une propriete topologique des applications globalement canoniques de la mechanique classique. *C. R. Acad. Sci.* 261:3719–22
2. Dombre T, Frisch U, Greene JM, Henon M, Mehr A, Soward AM. 1986. Chaotic streamlines in the ABC flows. *J. Fluid Mech.* 167:353–91
3. Aref H. 1984. Stirring by chaotic advection. *J. Fluid Mech.* 143:1–21
4. Strogatz SH. 2001. *Nonlinear Dynamics and Chaos: With Applications to Physics, Biology, Chemistry, and Engineering*. Cambridge, MA: Westview
5. Ranz WE. 1979. Application of a stretch model to mixing, diffusion, and reaction in laminar and turbulent flows. *AIChE J.* 25:41–47
6. Stroock AD, McGraw GJ. 2004. Investigation of the staggered herringbone mixer with a simple analytical model. *Philos. Trans. R. Soc. Lond. Ser. A* 362:971–86
7. McQuarrie DA. 2000. *Statistical Mechanics*. Sausalito, CA: Univ. Sci. Books
8. Aref H. 1983. Integrable, chaotic, and turbulent vortex motion in two-dimensional flows. *Annu. Rev. Fluid Mech.* 15:345–89
9. Ottino JM. 1990. Mixing, chaotic advection, and turbulence. *Annu. Rev. Fluid Mech.* 22:207–53
10. Wiggins S, Ottino JM. 2004. Foundations of chaotic mixing. *Philos. Trans. R. Soc. Lond. Ser. A.* 362:937–70
11. Solomon TH, Mezic I. 2003. Uniform resonant chaotic mixing in fluid flows. *Nature* 425:376–80
12. Rothstein D, Henry E, Gollub JP. 1999. Persistent patterns in transient chaotic fluid mixing. *Nature* 401:770–72
13. Bird RB, Stewart WE, Lightfoot EN. 2002. *Transport Phenomena*. New York: Wiley. 2nd ed.
14. Sturman R, Wiggins S. 2009. Eulerian indicators for predicting and optimizing mixing quality. *New J. Phys.* 11:075031
15. Stroock AD, Dertinger SKW, Ajdari A, Mezic I, Stone HA, Whitesides GM. 2002. Chaotic mixer for microchannels. *Science* 295:647–51
16. Schönfeld F, Hessel V, Hofmann C. 2004. An optimised split-and-recombine micro-mixer with uniform "chaotic" mixing. *Lab Chip* 4:65–69
17. Tabeling P, Chabert M, Dodge A, Jullien C, Okkels F. 2004. Chaotic mixing in cross-channel micromixers. *Philos. Trans. R. Soc. Lond. Ser. A* 362:987–1000
18. Qian SZ, Bau HH. 2002. A chaotic electroosmotic stirrer. *Anal. Chem.* 74:3616–25
19. Dean WR. 1928. Fluid motion in a curved channel. *Proc. R. Soc. Lond. Ser. A* 121:402–20
20. Sudarsan AP, Ugaz VM. 2006. Fluid mixing in planar spiral microchannels. *Lab Chip* 6:74–82
21. Groisman A, Steinberg V. 1998. Mechanism of elastic instability in Couette flow of polymer solutions: experiment. *Phys. Fluids* 10:2451–63
22. Groisman A, Steinberg V. 2001. Efficient mixing at low Reynolds numbers using polymer additives. *Nature* 410:905–8
23. Oddy MH, Santiago JG, Mikkelsen JC. 2001. Electrokinetic instability micromixing. *Anal. Chem.* 73:5822–32
24. Posner JD, Santiago JG. 2006. Convective instability of electrokinetic flows in a cross-shaped microchannel. *J. Fluid Mech.* 555:1–42
25. Paul EL, Atiemo-Obeng V, Kresta SM, eds. 2004. *Handbook of Industrial Mixing: Science and Practice*. Hoboken, NJ: Wiley
26. McCabe W, Smith J, Harriott P. 2004. *Unit Operations of Chemical Engineering*. New York: McGraw Hill
27. Lamberto DJ, Muzzio FJ, Swanson PD, Tonkovich AL. 1996. Using time-dependent RPM to enhance mixing in stirred vessels. *Chem. Eng. Sci.* 51:733–41

28. Wang W, Manas-Zloczower ICA, Kaufman M. 2005. Entropy time evolution in a twin-flight single-screw extruder and its relationship to chaos. *Chem. Eng. Commun.* 192:405–23
29. Hobbs DM, Muzzio FJ. 1997. The Kenics static mixer: a three-dimensional chaotic flow. *Chem. Eng. J.* 67:153–66
30. Stone HA, Stroock AD, Ajdari A. 2004. Engineering flows in small devices: microfluidics toward a lab-on-a-chip. *Annu. Rev. Fluid Mech.* 36:381–411
31. Stroock AD, Dertinger SK, Whitesides GM, Ajdari A. 2002. Patterning flows using grooved surfaces. *Anal. Chem.* 74:5306–12
32. Tice JD, Song H, Lyon AD, Ismagilov RF. 2003. Formation of droplets and mixing in multiphase microfluidics at low values of the Reynolds and the capillary numbers. *Langmuir* 19:9127–33
33. Song H, Bringer MR, Tice JD, Gerdts CJ, Ismagilov RF. 2003. Experimental test of scaling of mixing by chaotic advection in droplets moving through microfluidic channels. *Appl. Phys. Lett.* 83:4664–66
34. Bringer MR, Gerdts CJ, Song H, Tice JD, Ismagilov RF. 2004. Microfluidic systems for chemical kinetics that rely on chaotic mixing in droplets. *Philos. Trans. R. Soc. Lond. Ser. A* 362:1087–104
35. Leal GL. 1992. *Laminar Flow and Convective Transport Processes: Scaling Principles and Asymptotic Analysis*. Boston: Butterworth-Heinemann
36. Rhines PB, Young WR. 1983. How rapidly is a passive scalar mixed within closed streamlines? *J. Fluid Mech.* 133:133–45
37. Villermaux E, Stroock AD, Stone HA. 2008. Bridging kinematics and concentration content in a chaotic micromixer. *Phys. Rev. E* 77:4
38. Chertkov M, Lebedev V. 2003. Decay of scalar turbulence revisited. *Phys. Rev. Lett.* 90:034501
39. Lebedev VV, Turitsyn KS. 2004. Passive scalar evolution in peripheral regions. *Phys. Rev. E* 69:036301
40. Simonnet C, Groisman A. 2005. Chaotic mixing in a steady flow in a microchannel. *Phys. Rev. Lett.* 94:134501
41. Acharya N, Sen M, Chang HC. 1992. Heat-transfer enhancement in coiled tubes by chaotic mixing. *Int. J. Heat Mass Transf.* 35:2475–89
42. Chagny C, Castelain C, Peerhossaini H. 2000. Chaotic heat transfer for heat exchanger design and comparison with a regular regime for a large range of Reynolds numbers. *Appl. Therm. Eng.* 20:1615–48
43. Mokrani A, Castelain C, Peerhossaini H. 1997. The effects of chaotic advection on heat transfer. *Int. J. Heat Mass Transf.* 40:3089–104
44. Peerhossaini H, Castelain C, Leguer Y. 1993. Heat exchanger design based on chaotic advection. *Exp. Therm. Fluid Sci.* 7:333–34
45. Cohen JL, Volpe DJ, Westly DA, Pechenik A, Abruna HD. 2005. A dual electrolyte H_2/O_2 planar membraneless microchannel fuel cell system with open circuit potentials in excess of 1.4 V. *Langmuir* 21:3544–50
46. Ferrigno R, Stroock AD, Clark TD, Mayer M, Whitesides GM. 2002. Membraneless vanadium redox fuel cell using laminar flow. *J. Am. Chem. Soc.* 124:12930–31
47. Shrivastava A, Kumar S, Cussler EL. 2008. Predicting the effect of membrane spacers on mass transfer. *J. Membr. Sci.* 323:247–56
48. Brody JP, Yager P. 1997. Diffusion-based extraction in a microfabricated device. *Sens. Actuators Phys.* 58:13–18
49. Foley JO, Mashadi-Hossein A, Fu E, Finlayson BA, Yager P. 2008. Experimental and model investigation of the time-dependent 2-dimensional distribution of binding in a herringbone microchannel. *Lab Chip* 8:557–64
50. Golden JP, Floyd-Smith TM, Mott DR, Ligler FS. 2007. Target delivery in a microfluidic immunosensor. *Biosens. Bioelectron.* 22:2763–67
51. Kamholz AE, Weigl BH, Finlayson BA, Yager P. 1999. Quantitative analysis of molecular interaction in a microfluidic channel: the T-sensor. *Anal. Chem.* 71:5340–47
52. Squires TM, Messinger RJ, Manalis SR. 2008. Making it stick: convection, reaction and diffusion in surface-based biosensors. *Nat. Biotechnol.* 26:417–26
53. Vijayendran RA, Motsegood KM, Beebe DJ, Leckband DE. 2003. Evaluation of a three-dimensional micromixer in a surface-based biosensor. *Langmuir* 19:1824–28

54. Mary P, Studer V, Tabeling P. 2008. Microfluidic droplet-based liquid-liquid extraction. *Anal. Chem.* 80:2680–87
55. Bard AJ, Faulkner LR. 2001. *Electrochemical Methods: Fundamentals and Applications*. New York: Wiley
56. Kirtland JD, Stroock AD. 2011. Interfacial transfer from stirred laminar flows. In *Mixing in Laminar Fluid Flows: From Microfluidics to Oceanic Currents*, ed. RO Grigoriev, pp. 91–110. Weinheim, Germany: Wiley-VCH
57. Kirtland JD, McGraw GJ, Stroock AD. 2006. Mass transfer to reactive boundaries from steady three-dimensional flows in microchannels. *Phys. Fluids* 18:073602
58. Lévêque A. 1928. Les lois de la transmission de chaleur par convection. *Ann. Mines Mem.* 12 & 13:201–99, 305–62, 381–415
59. Kirtland JD, Siegel CR, Stroock AD. 2009. Interfacial mass transport in steady three-dimensional flows in microchannels. *New J. Phys.* 11:075028
60. Molho JI, Herr AE, Mosier BP, Santiago JG, Kenny TW, et al. 2001. Optimization of turn geometries for microchip electrophoresis. *Anal. Chem.* 73:1350–60
61. Obeid PJ, Christopoulos TK, Crabtree HJ, Backhouse CJ. 2003. Microfabricated device for DNA and RNA amplification by continuous-flow polymerase chain reaction and reverse transcription-polymerase chain reaction with cycle number selection. *Anal. Chem.* 75:288–95
62. Taylor G. 1953. Dispersion of soluble matter in solvent flowing slowly through a tube. *Proc. R. Soc. Lond. Ser. A* 219:186–203
63. Cantu-Perez A, Barrass S, Gavriilidis A. 2010. Residence time distributions in microchannels: comparison between channels with herringbone structures and a rectangular channel. *Chem. Eng. J.* 160:834–44
64. Jones SW, Young WR. 1994. Shear dispersion and anomalous diffusion by chaotic advection. *J. Fluid Mech.* 280:149–72
65. Koch DL, Brady JF. 1985. Dispersion in fixed beds. *J. Fluid Mech.* 154:399–427
66. Fountain GO, Khakhar DV, Ottino JM. 1998. Visualization of three-dimensional chaos. *Science* 281:683–86
67. Berg HC. 1993. *Random Walks in Biology*. Princeton, NJ: Princeton Univ. Press
68. Wang L, Li PCH. 2011. Microfluidic DNA microarray analysis: a review. *Anal. Chim. Acta* 687:12–27
69. Hertzsch JM, Sturman R, Wiggins S. 2007. DNA microarrays: design principles for maximizing ergodic, chaotic mixing. *Small* 3:202–18
70. McQuain MK, Seale K, Peek J, Fisher TS, Levy S, et al. 2004. Chaotic mixer improves microarray hybridization. *Anal. Biochem.* 325:215–26
71. Aref H, Jones SW. 1989. Enhanced separation of diffusing particles by chaotic advection. *Phys. Fluids A* 1:470–74
72. Vergassola M, Villermaux E, Shraiman BI. 2007. "Infotaxis" as a strategy for searching without gradients. *Nature* 445:406–9

Annual Review of Chemical and Biomolecular Engineering

Volume 3, 2012

Contents

Indexes

Errata

An online log of corrections to *Annual Review of Chemical and Biomolecular Engineering* articles may be found at http://chembioeng.annualreviews.org/errata.shtml